Development of new processes to protect zinc against corrosion, suitable for on-site use

Vincent Meiffren, Kevin Dumont, Pascal Lenormand, Florence Ansart*, Stephan Manov

CIRIMAT – UMR CNRS 5085, 119 route de Narbonne, 31062 Toulouse, France

Keywords:
Sol–gel
Protective coatings
Hybrid coatings
Corrosion
Industrial transfer

A B S T R A C T

Protection against corrosion of metals is well known as an important issue in numerous fields. In all cases, the improvement of durability of these metals has to be connected to the development of environmentally friendly processes. Sol–gel protective coatings have shown excellent chemical stability and enhanced corrosion resistance for zinc substrates. Further, the sol–gel method, used as technique of surface protection, showed the potential for the replacement of toxic pre-treatments. This paper highlights the recent developments and applications of silane based sol–gel coatings on zinc substrates. Then, the challenges for industrial transfer of the developed process are also discussed because this process presents a disadvantage for on-site use, which is the too time-consuming thermal treatment. So, the goal of this study was to determine the convenient experimental conditions to reduce the duration of heat treatment of the hybrid sol–gel layer, compatible with the severe industrial requirements, without reducing the protection against corrosion. To reach this objective, a correlation between the results of chemical analyses and the protection against corrosion efficiency was established.

1. Introduction

Most metals need to be protected against corrosion to slow down and limit the effects of time. For instance, the surface of zinc metal spontaneously reacts with the atmosphere (e.g. O_2, H_2O, CO_2) to produce protective corrosion compounds such as zinc hydroxycarbonate (natural patina) which decreases the progress of corrosion. But in some cases, species contained in the atmosphere (such as chlorides or sulfides) can react with the substrate and lead to the formation of white rust. Several treatments are already available to tackle this issue such as chemical conversion (phosphatation or chromatation).

Drastic new regulations and improvements in know-how have led to the development of more environmentally friendly processes for metal protection. Metal corrosion studies have shown the feasibility of efficient protection via a new eco-friendly route called sol–gel [1–5]. It consists of the hydrolysis and condensation of metal alkoxides to obtain metaloxane chains [6–9]. These chains generate sols that are then used to coat numerous metal substrates to protect them against corrosion [1–6,10–14].

Commonly, sol–gel processes involve silane precursors as starting materials. In this study, we report good performance in terms of corrosion resistance with an organic–inorganic sol–gel process. Raw compounds, ASB (aluminum-tri-sec butoxide) and GPTMS (3-glycidoxypropyltrimethoxysilane) are mixed in propan-2-ol and then water containing a corrosion inhibitor [15–20] (cerium III nitrate hexahydrate) is added. This process appeared efficient, but the drying step is not very compatible with industrial transfer requirements because it is too time-consuming (36 h). Preliminary tests have shown that reducing the heating time decreases corrosion protection. So the drying temperature had to be optimized to reduce the duration of heat treatment.

To reach this goal, different drying temperatures were used for 1 h. FTIR spectroscopy was used on xerogels to identify the influence of heat treatment on chemical reactions. The aim was to know if it was possible to obtain an equivalent polymeric network with shorter thermal treatment. Then, microstructural observations were performed on sample cross sections to check that all coatings were regular and with comparable thickness. Then, accelerated corrosion testing and electrochemical analysis were carried out to correlate microstructural and chemical characteristics to corrosion protection efficiency.

2. Materials and methods

2.1. Samples preparation

Rolled and mechanically brushed zinc strip (0.7 mm thick) was used as substrate. Samples (25 mm × 80 mm) were cut and cleaned with ethanol, and then immersed in a commercial alkaline

* Corresponding author. Tel.: +33 561556108.
E-mail address: ansart@chimie.ups-tlse.fr (F. Ansart).

doi:10.1016/j.porgcoat.2011.03.025

solution (Novaclean®) for 5 min at 80 °C to remove the oxide layer and improve wettability. In these conditions, the cleaned zinc has an average roughness (Ra) of 0.6 μm.

Sol–gel solution was obtained by mixing Solution A, which was composed of the commercial precursors GPTMS (3-glycidoxypropyltrimethoxysilane) and ASB (aluminum-tri-sec butoxide) (provided by Aldrich) in propan-2-ol in a 7:3:3 molar ratio and Solution B which was water containing 2×10^{-2} mol/L of cerium nitrate hexahydrate (purchased from Acros). The mixed solutions A and B were vigorously stirred to obtain a clear liquid. Furthermore, before deposition, the solution was aged for 24 h to let sol–gel reactions become initiated. Two reactions play a key role in the sol–gel transition, the initiation step (hydrolysis) which consists in the formation of M–OH bonds (reaction 1) then the propagation step (condensation) which leads to M–O–M bond formation (reaction (2)) [6,7].

$$\text{Hydrolysis}: R'M(OR)_n + nH_2O \rightarrow R'M(OH)_n + nR{-}OH \quad (1)$$

$$\text{(2) Condensation: } R'M(OH)_n + R'M(OH)_n \rightarrow R'\text{-}\underset{(HO)_{n-1}}{\overset{}{M}}\text{-O-}\underset{(HO)_{n-1}}{\overset{}{M}}\text{-}R' + H_2O \quad (2)$$

$$\text{(2') Condensation: } R'M(OH)_n + R'M(OR)_n \rightarrow R'\text{-}\underset{(HO)_{n-1}}{\overset{}{M}}\text{-O-}\underset{(OR)_{n-1}}{\overset{}{M}}\text{-}R' + R\text{-}OH$$

$$R=CH_3;\ CH(CH_3)\ \ (C_2H_5),\ \ R'=\text{alkyl group and } M=Si;\ Al \quad (2')$$

The matured sol was then dip-coated onto zinc substrate at a controlled withdrawal rate of 20 cm/min. One advantage of this technique is that several chemical bonds are formed even between the surface and the inorganic network $M_{network}$–O–$M_{substrate}$. They form between the sol–gel matrix and the zinc substrate [6–8,21] which increase anchorage of the coating to the metal surface. After deposition, coated samples were dried for 20 h at 50 °C followed by 16 h at 110 °C to remove organic solvents (alcohols) and water, and to catalyze condensation reactions.

2.2. Characterization of sol–gel coating

First, xerogel was chemically analyzed by FTIR spectroscopy to determine precisely which bonds are involved. The xerogel was obtained by drying a few milliliters of the sol–gel solution at room temperature. Then, to perform FTIR analysis of the coatings, glass strips were coated in the same conditions as the zinc thus avoiding contamination of the coating by the metal. KBr pellets containing 1%$_{wt}$ of the ground powder of the sol–gel coating were then analyzed using a Bruker Vector 22 apparatus. FTIR Spectra were collected in the 400–4000 cm^{-1} range.

Then, to evaluate coating conformity macrostructural properties, SEM observations were performed on sample sections with a JEOL JSM-6510LV apparatus. Before metallization, samples were cut perpendicularly to the rolled side and embedded in resin, before polishing to ¼ μm.

Finally, anticorrosion properties were investigated both macroscopically and microscopically. Firstly they were evaluated during a Q-fog cyclic corrosion test which is a conventional industrial test. Test duration was kept constant: 10 cycles, 24 h each. One cycle consists in different steps alternating wet and dry atmospheres at different temperatures. During the moisture stage, the chamber was maintained at near 100% relative humidity. In order to quantify white rust formation, the samples were weighed before and after each corrosion cycle.

Secondly, EIS measurements were performed to highlight protection mechanisms of coated samples. The analyzed areas always covered an area of exactly 5 cm^2. The impedance measurements were carried out after 1 h of immersion in a 0.5 mol/L Na_2SO_4 electrolyte and recorded over a frequency range between 65 kHz and 100 mHz with an amplitude of 10 mV. Both Bode and Nyquist plots were used to compare sample behavior.

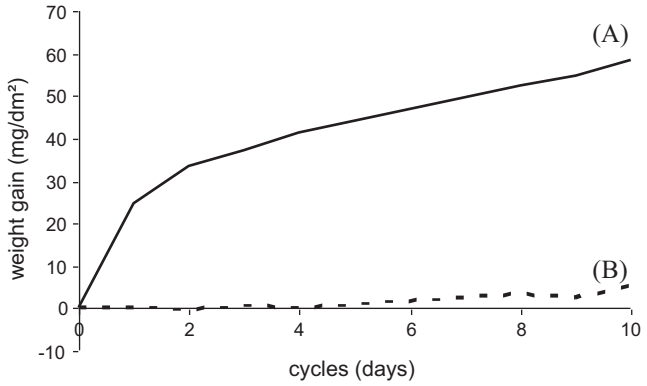

Fig. 1. Weight gain of (A) uncoated zinc and (B) coated zinc over 10 days in the cyclic humidity chamber.

3. Results and discussion

3.1. Characteristics of the first GPTMS/ASB coating

The starting point of this study was the very good anticorrosive property of a sol–gel coating obtained mixing GPTMS and ASB with cerium nitrate as corrosion inhibitor and dried for 20 h at 50 °C followed by 16 h at 110 °C. These characteristics are indicated below and high protective properties were also identified by an industrial macroscopic corrosion test and electrochemical analyses.

3.1.1. Accelerated corrosion test

In order to evaluate the resistance against corrosion of coated zinc, normalized cyclic humidity tests were carried out. This test is representative of the layer's behavior in natural corrosive atmosphere. To insure the suitability of the test, three uncoated samples and three coated samples were placed in the humidity chamber. Afterwards, all samples were weighed after each cycle. The weight variations over 10 days are reported in Fig. 1. The weight gain for uncoated substrate increased strongly during the first cycle, but after the second cycle the oxidation kinetic slowed down and the weight gain increased slightly to finish at around 60 mg/dm^2 at the end of the test. For coated substrate, the weight gain was much lower (5 mg/dm^2) indicating a significant decrease of oxidation. In fact, white rust formation was strongly delayed. In addition, macrographs after 1, 4 and 10 days (Fig. 2.) showed that for uncoated samples, the surface is entirely covered by corrosion products from the fourth cycle. For coated samples, white rust only appeared as small areas on the edges (edge effect). This test proves the effectiveness of corrosion protection of hybrid coatings applied on zinc substrate.

3.1.2. Electrochemical analyses

EIS analyses were performed on uncoated and coated zinc substrates to evaluate influence of the hybrid coating on the electrical behavior of zinc. Nyquist (Fig. 3.) and Bode (Fig. 4.) patterns were plotted in order to determine the benefits of the sol–gel layer. The Nyquist complex plane of the uncoated substrate exhibits one small capacitive loop attributed to the thin zinc oxide film with a resistance around 200 Ω cm^2. But concerning coated zinc, a first well defined capacitive semicircle with a resistance near 170 kΩ cm^2 was assigned to ionic resistance of the coating [10,16,22]. This large increase of impedance clearly shows the protective efficiency of the layer barrier effect.

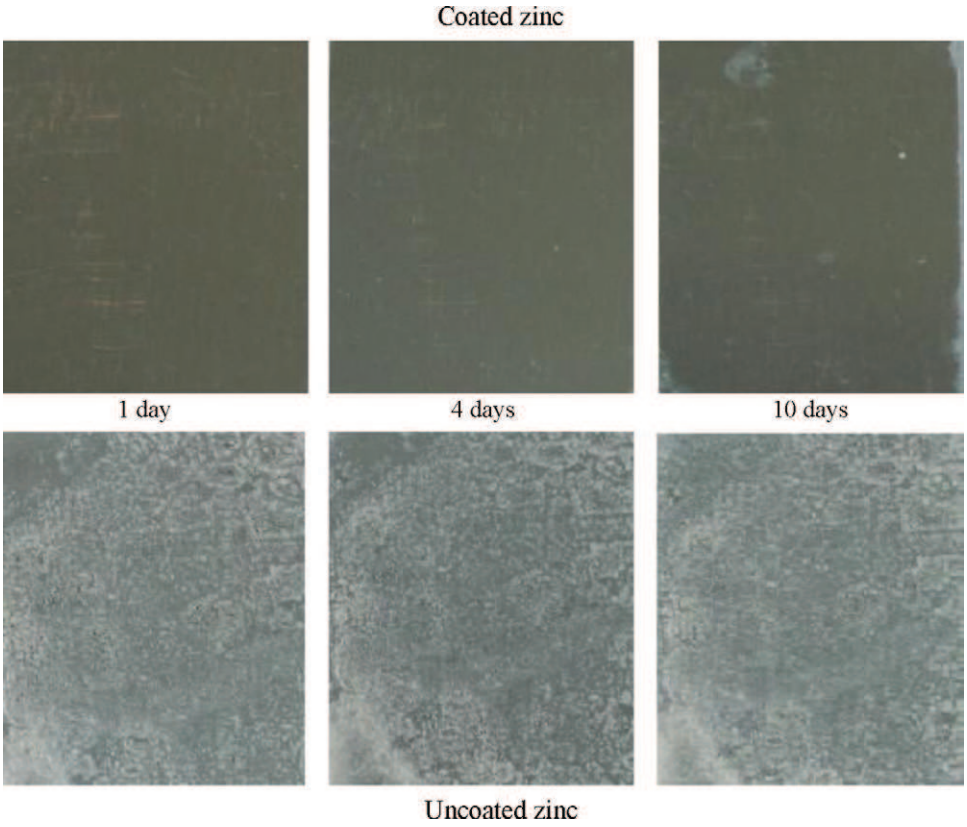

Fig. 2. Samples of coated and uncoated zinc after 1 day, 4 days and 10 days in the cyclic humidity chamber.

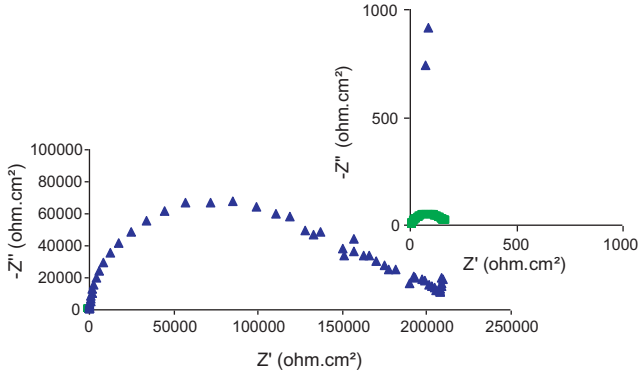

Fig. 3. Nyquist representation of uncoated samples (■) and coated samples (▲) after 1 h of immersion in Na_2SO_4.

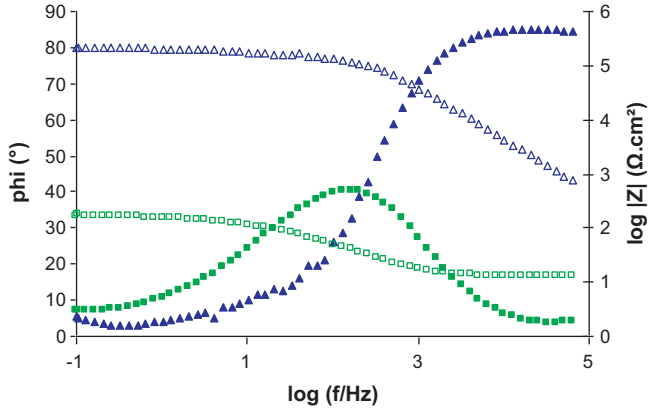

Fig. 4. Phase angle of uncoated samples (■) and coated samples (▲) and log |Z| of uncoated samples (□) and coated samples (△) after 1 h of immersion in Na_2SO_4 versus frequency.

Bode representation highlights the capacitance of the sol–gel film at high frequencies (10^4–10^5 Hz). Furthermore, the phase is around 85° showing the strong barrier effect of the layer. Moreover, the increase of the resistive plateau of about 2 orders of magnitude higher at 1 Hz focuses on the great improvement of barrier effect.

Both tests show the high efficiency of sol–gel protection by this process, but the process cannot be successfully transferred at an industrial scale due to the long heating times required. So, the main objective is to simplify the thermal treatment process from the point of view of both temperature and time. But the challenge is to preserve the same anti-corrosion performances.

3.2. Reduction of the drying time

In our case, the technological bottle-neck remained the drying step in terms of time and temperature, because the end point should be the transfer of this process to the production line. So, classical drying should be replaced by a shorter one. The first part of this work identified the chemical reactions due to thermal treatment. Nevertheless, to understand which chemical reactions are involved, some preliminary analyses were carried out. Indeed, spectra of pure GPTMS collected in liquid media and xerogel dried at room temperature were recorded in KBr tablets (Fig. 5.).

The analysis of the GPTMS spectra revealed two bands centered at around 2940 cm^{-1} and 2840 cm^{-1} corresponding respectively to asymmetric and symmetric C–H stretching of methoxy groups and CH_2 of the organic chain of GPTMS [23]. Furthermore, C–H deformation appears around 1195 cm^{-1} [23] and intense bands centered at 1085 cm^{-1} and 815 cm^{-1} are attributed to Si–O in Si–O–CH_3 asymmetric and symmetric stretching vibration [23]. Several vibrational frequencies due to the epoxy part of glycidoxypropylsiloxane are also attributed to epoxy ring breathing at around 1275 cm^{-1}, asymmetric epoxide ring deformation at 905 cm^{-1} and 780 cm^{-1} and C–O twist vibration nearly 850 cm^{-1} [21,23].

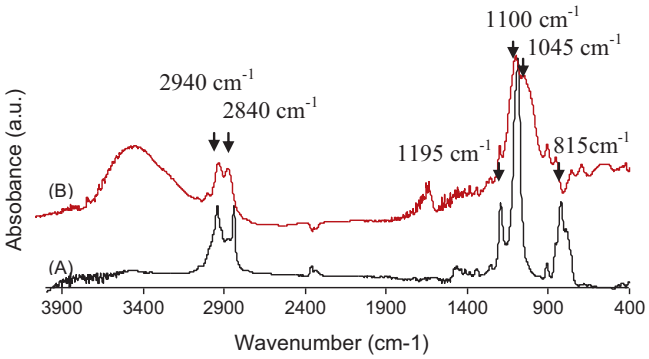

Fig. 5. FTIR spectra performed on pure GPTMS (A), xerogel (B).

It is important to underline that, in the xerogel spectra, peaks attributed to C–H in methoxy groups are less intense, which means that hydrolysis occurs. But, stretching vibrations of the silanol Si–OH at around 960 cm^{-1} [24] were not observed. The very intense bands appearing at 1100 cm^{-1} and 1045 cm^{-1} are due to both Si–O–Si and Si–O–C stretching vibrations [25] which indicates that condensation of silanol has been achieved. Therefore, these analyses confirm the Si–O–Si network formation by this process.

Then, in order to understand the effect of various thermal treatments towards chemical reactions, layers were deposited on glass substrates and dried at different temperatures. According to the thermo-gravimetric analysis of the xerogel, the drying temperature has to be lower than 260 °C to avoid alterations of the organic compounds. So, we defined several temperatures below this value: 80 °C, 110 °C, 130 °C, 150 °C, 180 °C and the standard drying (20 h at 50 °C followed by 16 h at 110 °C). As the goal was to check if a shorter heat treatment (1 h) could be equivalent to the conventional long heat treatment, we plotted FTIR spectra, which are reported in Fig. 6.

It is worth noting that all bands are present in each case but some bands appear more intense with lower drying temperatures. In fact, above 130 °C peaks only appear as shoulders. These bands are centered on the following wavelengths: 1275 cm^{-1}, 905 cm^{-1}, 850 cm^{-1} and 780 cm^{-1} (typical epoxy ring bands).

However, acid medium catalyzes the reaction of epoxy ring with water forming hydroxyl groups. In our case, the sol is slightly acidified by nitrates from the cerium nitrate (pH = 4.5). So, epoxy rings are able to open and to polymerize into a linear poly(ethylene oxide) organic network [21]. But, a linkage between Si–OH and Al–OH (hydrolyzed species) with the opened epoxy ring can also occur [25]. The effect of these bonds will increase the number of branches in the network. On the other hand, bands assigned to Si–O–C and Al–O are present in the range 1100 cm^{-1} to 1000 cm^{-1} [25,26]. But their positions are similar to the Si–O–Si stretching vibration. So it is difficult to conclude.

Table 1
Average weight gain of all samples.

Drying	Layer weight gain (mg/dm²)
80 °C – 1 h	43
110 °C – 1 h	43
130 °C – 1 h	44
150 °C – 1 h	43
180 °C – 1 h	43
Standard drying	47

Nevertheless, we can add that similar organic–inorganic bonds at respectively 150 °C, 180 °C and for the standard drying can be observed. So, the chemical mechanism seems to be identical for the three heat treatments, which means that the chemical skeleton is the same in the matrix.

But, even though chemical bonds are similar, the microstructure was observed by electronic microscopy to investigate the effect of the treatment on the coating and the interface. Because it is well known that sol–gel coatings confer barrier effect protection to metallic substrates [6], and that the barrier effect of the sol–gel layer is directly correlated to microstructural parameters such as thickness, covering ability, porosity, microscopy observations were carried out on cross-sections and surfaces of samples for all heat treatments to determine their thickness, ability to form a suitable coating and if the topography was properly covered by the layer. Figs. 7a and 8a respectively show the cross section of a sample heated to 180 °C and one cured by standard heat treatment: all cross sections appear similar. As can be seen, both samples presented similar average coating thickness. Surfaces of these samples are reported on Figs. 7b and 8b and no difference can be noted. Coatings are continuous and they are crack free. Bright areas indicate substrate vicinity showing the high roughness of zinc strips.

For all drying conditions, the surface roughness of the substrate was not reproduced by the film and adhesion was good, as proved by industrial tests ISO 2409 and 6272. The average thickness of the films was evaluated at 3 μm but the local thickness was strongly dependant on the substrate roughness.

Furthermore, all weight gains, compiled in Table 1, were similar whatever the drying treatment. This point indicates that organic solvents were removed in all cases.

Corrosion tests were then performed: three samples were dipped into the sol–gel solution and after controlled withdrawal, dried at different temperatures as described previously and in parallel with the standard drying. Then, all samples were placed in the cyclic humidity test device with three blank substrates. Weight gains during 10 cycles, reported in Fig. 9, show similar weight increases for all samples except those dried at 80 °C. For this lower

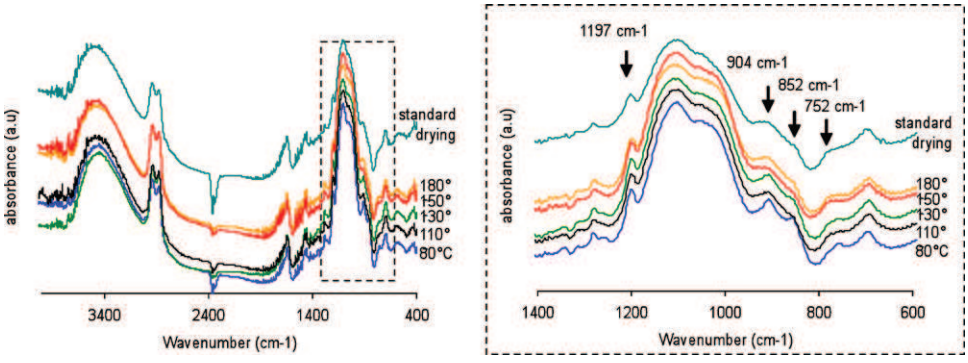

Fig. 6. FTIR spectra obtained on ground powder of coatings dried with each heat treatment.

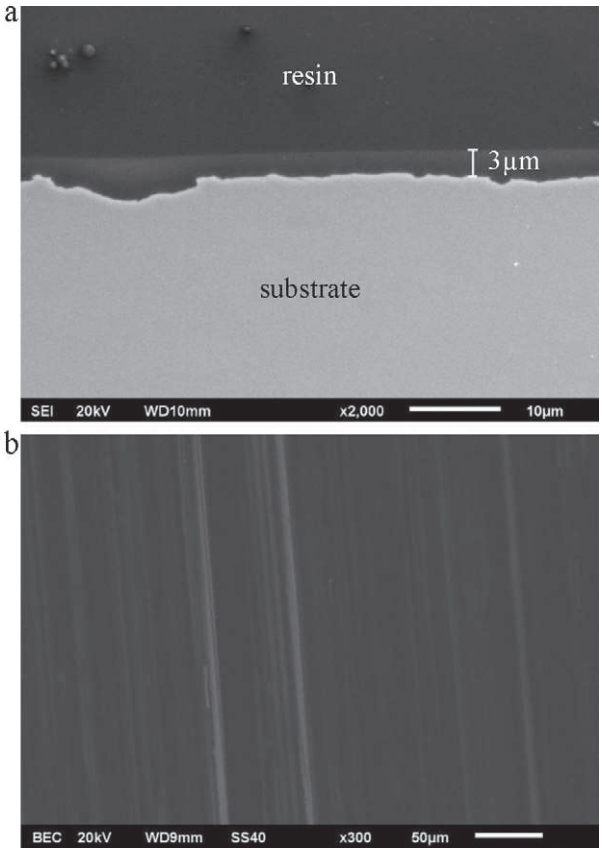

Fig. 7. (a) Cross section of coated zinc dried 20 h at 50 °C followed by 16 h at 110 °C, observed by secondary electron microscopy (b) surface of coated zinc dried 20 h at 50 °C followed by 16 h at 110 °C, observed by back-scattered electron microscopy.

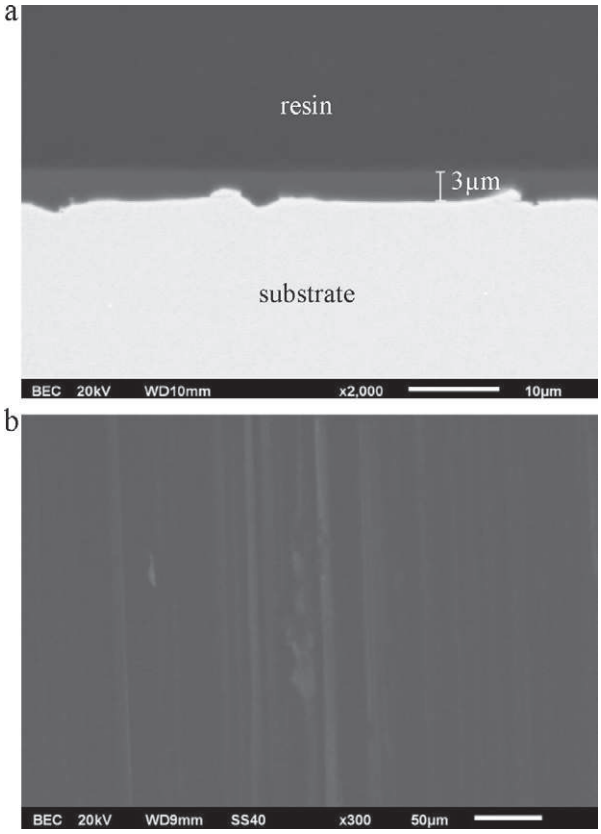

Fig. 8. (a) Cross section of coated zinc cured at 180 °C for 1 h observed by back-scattered electron microscopy (b) Surface of coated zinc cured at 180 °C for 1 h observed by back-scattered electron microscopy.

temperature of drying we observe a weight decrease attributed to the loss of matter due to edge effects.

For samples dried at 110 °C and 130 °C edge cracks led to decreases in weight gain due to loss of coating fragments. Moreover, for samples cured at 150 °C and 180 °C for 1 h, very small areas were damaged, as for the sample with standard drying. So, we can consider that the protection efficiency after these drying tests was roughly similar (Fig. 10).

To correlate macroscopic observations after accelerated corrosion test with electrochemical properties, EIS measurements were performed. This technique enables the oxidation phenomena to be separated. In the Nyquist plot in Fig. 11, several capacitive loops are observed for each sample. At high frequencies, the first well defined loop, assigned to ionic resistance of the coating significantly increases for higher temperatures: around 750 $\Omega\,cm^2$ for the sample dried at 80 °C, 15 $k\Omega\,cm^2$ for 110 °C, 75 $k\Omega\,cm^2$ for 130 °C and 150 °C and near 200 $k\Omega\,cm^2$ for the 180 °C sample. Considering loops at lower frequencies, phenomenon may correspond to ion-electron charge transfer arising from the corrosion reaction at the interface coating/substrate [16]. The charge transfer semicircle is better defined when the pore resistance is low as we can see on the zoom (Fig. 11). The cooler the heat treatment is, the better defined is the electrochemical response at low frequencies. This indicates that the charge transfer kinetics are strongly reduced.

Concerning Bode representation on Fig. 12, a shift to high impedance of the plateau resistance is observed for higher temperatures which can be correlated to the greater density of cross-links in the film. Furthermore the phase difference indicates the presence of a large capacitance to high frequencies (10^4–10^5 Hz) for coated samples. This high phase difference was more spread out for higher treatment temperatures: a phenomenon that can be attributed to the barrier effect.

Then, the zinc oxide film response is not clearly seen for thermal treatment over 110 °C indicating a slowing down of zinc oxidation kinetics. Moreover, substrate oxidation was not totally stopped but the decrease is sufficient to satisfy industrial specifications.

From these results, a correlation can be made between the results of the accelerated corrosion test and the EIS measurement. Indeed, samples showing greater protection in the corrosion test had a larger capacitive loop, a higher resistance

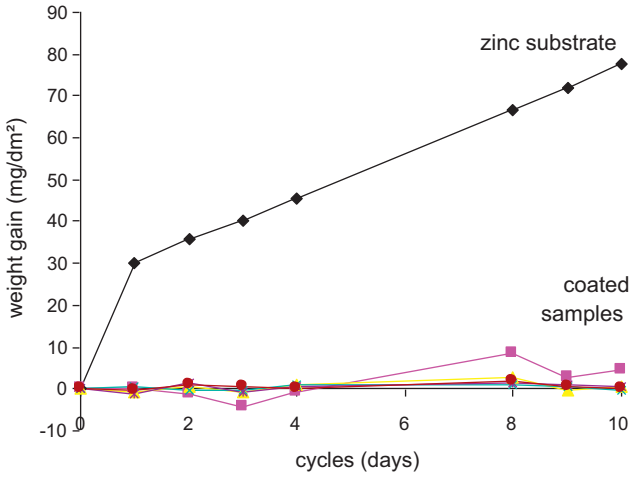

Fig. 9. Weight gain for zinc substrate and coated samples.

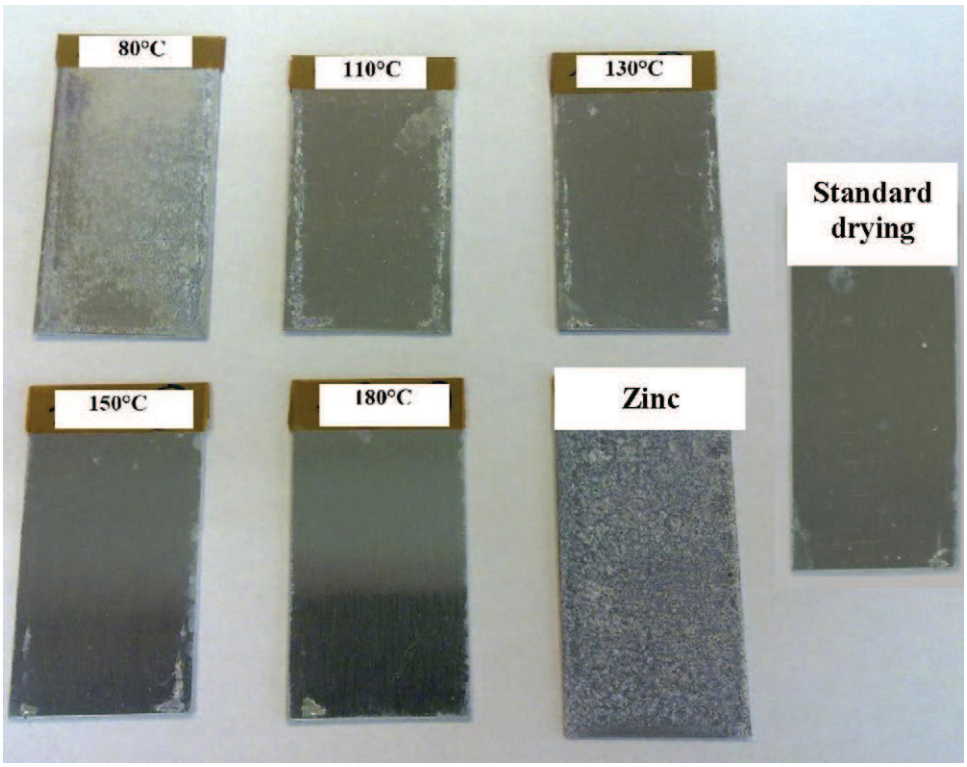

Fig. 10. Tested samples after 10 cycles.

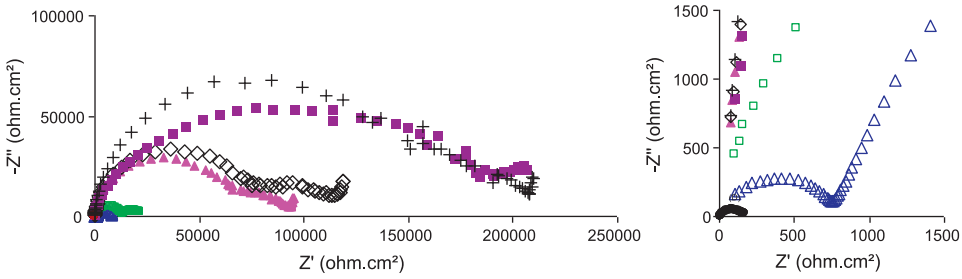

Fig. 11. Nyquist plot after 1 h of immersion in a 0.5 M Na_2SO_4 solution of zinc substrate (●), 80 °C dried sample (△), 110 °C (□), 130 °C (▲), 150 °C (◊), 180 °C (■) and (+) for standard dried sample.

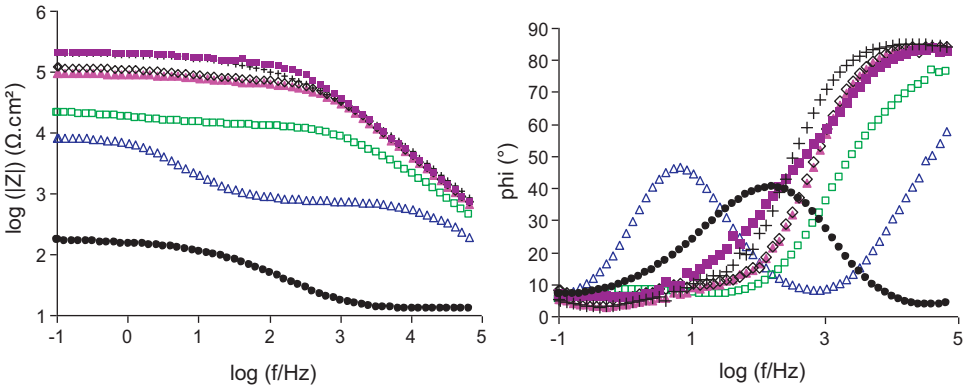

Fig. 12. Bode representation plotted after 1 h of immersion of zinc substrate in a 0.5 M Na_2SO_4 solution (●), 80 °C dried sample (△), 110 °C (□), 130 °C (▲), 150 °C (◊), 180 °C (■) and (+) for standard dried sample.

plateau and showed capacitive behaviour over a greater range of frequencies.

4. Conclusion

The goal of this study was to reduce the duration of heat treatment of the hybrid sol–gel layer without reducing the protection against corrosion. A correlation between the results of chemical analyses and the protection against corrosion efficiency was demonstrated. Indeed, FTIR spectroscopy showed similarities in epoxy ring opening between 150 °C, 180 °C and standard thermal treatment. Furthermore, cyclic humidity tests showed very good corrosion protection for the three thermal treatments. In fact, low weight gain was observed after 10 cycles, with very little white rust. In addition, EIS measurements underlined the very similar resistance of the first capacitive loop in the sample dried following the standard lower temperature and slower procedure and one dried at 180 °C. Moreover, Bode representation of both drying types revealed similar resistance of the coating pores. Considering these results, standard drying can easily be replaced by heat treatment for 1 h at 180 °C.

The second conclusion of this work is the establishment of a link between epoxy ring opening and corrosion protection efficiency. In fact, increasing the number of epoxy rings that open leads to a more branched network. Consequently, the penetration of corrosive species into coating pores decreases (increase of barrier effect). This phenomenon slows down the oxidation of the zinc substrate. EIS measurements showing the improvement of ionic resistance of the coating pores corroborated this hypothesis. However, further analyses planned including NMR or Raman spectroscopy should indicate exactly which bonds are formed following epoxy ring opening.

References

[1] S. Pathak, A. Khanna, Progress in Organic Coatings 62 (2008) 409–416.
[2] N. Voevodin, V. Balbyshev, M. Donley, Progress in Organic Coatings 52 (2005) 28–33.
[3] A.S. Hamdy, D. Butt, Surface and Coatings Technology 201 (2006) 401–407.
[4] R.L. Parkhill, E.T. Knobbe, M.S. Donley, Progress in Organic Coatings 41 (2001) 261–265.
[5] Y. Li, A. Ba, M.S. Mahmood, Electrochimica Acta 53 (2008) 7859–7862.
[6] D. Wang, G.P. Bierwagen, Progress in Organic Coatings 64 (2009) 327–338.
[7] C.J.N.L. Brinker, G.W.D.P.D.N.A.C. Scherer, Sol–Gel Science (1990).
[8] Y. Joshua Du, M. Damron, G. Tang, H. Zheng, C.-J. Chu, J.H. Osborne, Progress in Organic Coatings 41 (2001) 226–232.
[9] C. Brinker, G. Frye, A. Hurd, C. Ashley, Thin Solid Films 201 (1991) 97–108.
[10] X. Zhong, Q. Li, J. Hu, S. Zhang, B. Chen, S. Xu, F. Luo, Electrochimica Acta 55 (2010) 2424–2429.
[11] V. Sarmento, M. Schiavetto, P. Hammer, A. Benedetti, C. Fugivara, P. Suegama, S. Pulcinelli, C. Santilli, Surface and Coatings Technology 204 (2010) 2689–2701.
[12] A.L.K. Tan, A.M. Soutar, Thin Solid Films 516 (2008) 5706–5709.
[13] A. Galio, S. Lamaka, M. Zheludkevich, L. Dick, I. Müller, M. Ferreira, Surface and Coatings Technology 204 (2010) 1479–1486.
[14] W.E. Hansal, S. Hansal, M. Pölzler, A. Kornherr, G. Zifferer, G.E. Nauer, Surface and Coatings Technology 200 (2006) 3056–3063.
[15] K. Aramaki, Corrosion Science 43 (2001) 2201–2215.
[16] M. Garcia-Heras, A. Jimenez-Morales, B. Casal, J.C. Galvan, S. Radzki, M.A. Villegas, Journal of Alloys and Compounds 380 (2004) 219–224.
[17] X. Yue, L. Yingjie, L. Sha, Journal of Rare Earths 25 (2007) 193–196.
[18] P. Hammer, M.G. Schiavetto, F.C. dos Santos, A.V. Benedetti, S.H. Pulcinelli, C.V. Santilli, Journal of Non-Crystalline Solids 356 (2010) 2606–2612.
[19] N. Rosero-Navarro, M. Curioni, R. Bingham, A. Durán, M. Aparicio, R. Cottis, G. Thompson, Corrosion Science 52 (2010) 3356–3366.
[20] M.F. Montemor, A.M. Simões, M.G.S. Ferreira, Progress in Organic Coatings 44 (2002) 111–120.
[21] R. Zandi-zand, A. Ershad-langroudi, A. Rahimi, Progress in Organic Coatings 53 (2005) 286–291.
[22] S. Pathak, A. Khanna, Progress in Organic Coatings. 62 (2008) 409–416.
[23] I.M. Sapic, L. Bistricic, V. Volovsek, V. Dananic, K. Furic, Spectrochimica Acta Part A: Molecular and Biomolecular Spectroscopy 72 (2009) 833–840.
[24] R. Al-Oweini, H. El-Rassy, Journal of Molecular Structure 919 (2009) 140–145.
[25] R. Guo, C. Hu, F. Pan, H. Wu, Z. Jiang, Journal of Membrane Science 281 (2006) 454–462.
[26] T. Meher, A. Basu, S. Ghatak, Ceramics International 31 (2005) 831–838.